

Electrochemical characterization of platinum–ruthenium nanoparticles prepared by water-in-oil microemulsion

J. Solla-Gullón*, F.J. Vidal-Iglesias, V. Montiel¹, A. Aldaz¹

Departamento de Química-Física, Universidad de Alicante, Instituto Universitario de Electroquímica, Apartado 99, 03080 Alicante, Spain

Received 3 March 2004; received in revised form 14 May 2004; accepted 10 June 2004

Available online 17 July 2004

Abstract

The synthesis, physical characterization, decontamination and some electrocatalytic properties of PtRu nanoparticles prepared using the microemulsion method are reported. The nanoparticles are synthesized by reduction with sodium borohydride of H_2PtCl_6 and RuCl_3 in a water-in-oil microemulsion of water/polyethyleneglycol-dodecylether (BRIJ[®] 30)/*n*-heptane. X-ray diffraction (XRD), X-ray photoelectron spectroscopy (XPS), transmission electron microscopy (TEM) and energy dispersive analysis by X-rays (EDAX) experiments were carried out to characterize the single and bimetallic nanoparticles obtained. Cyclic voltammograms (CV) of clean nanoparticles were obtained after a controlled decontamination procedure of their surfaces. CO adsorption–oxidation and methanol electrooxidation were used as test reactions to check the electrocatalytic behaviour of the bimetallic nanoparticles. Pt₈₀Ru₂₀ (nominal atomic composition) nanoparticles are the best electrocatalyst for both CO_{ad} and methanol oxidation. All these results show that the microemulsion method can be used to produce bimetallic nanoparticles in a very easy way. The method can be very easily scaled-up for industrial use.

© 2004 Elsevier Ltd. All rights reserved.

Keywords: Nanoparticles; Microemulsion; Pt-Ru catalyst; Methanol oxidation; Fuel cells

1. Introduction

Despite the search of new catalytic materials for fuel cell systems, PtRu alloys still remain the best choice as anode catalyst for low-temperature polymer electrolyte fuel cells (PEFC) both for PEFCs operated by H₂-rich reformat or for PEFCs driven by direct oxidation of methanol (DMFC). Anyway, and in both cases, the main problem is related to the gradual poisoning of the catalyst by CO due to the presence of CO trace impurities in the reformat or by CO formation during the methanol dehydrogenation. The superior activity of PtRu against other catalytic materials has been explained by a bifunctional mechanism where the oxidation of adsorbed CO is facilitated by the presence of –OH_{ad} species formed at low anodic overpotentials on oxophilic surface atoms such as Ru [1,2]. In addition, it should be pointed out

that the so-called ligand or electronic effect might also be involved in the process [3,4]. In both cases, the catalyst composition and specially its surface composition should play a fundamental role on its electrocatalytic behaviour. Thus, although this fact has been demonstrated for CO and methanol oxidation in model studies on different PtRu electrodes, —massive PtRu alloys, PtRu surface alloys, Ru modified Pt electrodes and high surface area carbon supported and unsupported PtRu catalysts [5–12]—, in the case of high surface area catalysts (nanoparticles), systematic studies of the influence of the atomic composition are still in continuous progress.

Nanoparticles are very adequate as electrocatalysts for fuel cell and recent years have witnessed an increasing interest on new synthesis methods that could be easily translated to applied scale. Since the platinum-group metal nanoparticles were synthesized in a water-in-oil microemulsion by Boutonnet et al. [13], the microemulsion technique has been used to prepare a great number of nanomaterials such as pure metals [13,14], alloys [14–16], metal borides

* Corresponding author. Fax: +34 965 903537.

E-mail address: jose.solla@ua.es (J. Solla-Gullón).

¹ ISE member.

[17], metal oxides and hydroxides [18–23], organic polymers [24], etc. However and in spite of the fact that it is a very easy and reproducible technique, very few works have been devoted to the use of this method to synthesize nanoparticles to be used as electrocatalyst [25–27]. From an electrochemical point of view, the key problem of the synthesis of nanoparticles in microemulsion is that the nanoparticles obtained are coated with a film of surfactant molecules that blocks the surface sites, modifying their surface properties and particularly their electrocatalytic properties. For that reason, in previous works, we have developed some procedures to clean, without surface damage or composition changes, Pt, Pd and Pt/Pd alloy nanoparticles prepared with this methodology [25,28–30].

The aim of this paper is to show that the microemulsion technique allows the fabrication of bimetallic nanoparticles of Pt/Ru in a very easy way and with similar electrocatalytic activity to that obtained using more elaborated methods. Moreover, this method can be very easily scaled-up for industrial applications. Thus, in this paper we present recent results about the synthesis, physical characterization, decontamination and some electrocatalytic properties of PtRu nanoparticles prepared in microemulsion.

2. Experimental

2.1. Preparation and characterization of nanoparticles

Platinum and ruthenium nanoparticles were obtained by reduction of either H_2PtCl_6 or RuCl_3 with sodium borohydride using a w/o microemulsion of water/polyethylenglycol-dodecylether (BRIJ[®] 30)/*n*-heptane. The size of the microemulsion droplet is determined by the molar ratio of water to surfactant (ω_0). The concentration of surfactant, in volume, amounts in this work to 16.5% of the total microemulsion volume. The concentrations of H_2PtCl_6 and RuCl_3 solutions employed for the synthesis were 0.1 M. For the preparation of alloyed nanoparticles, an aqueous solution of $\text{H}_2\text{PtCl}_6 + \text{RuCl}_3$ with the convenient atomic proportion of the two elements was employed. In order to have micelles with the same size, i.e. nanoparticles within the same size range, the molar ratio water to surfactant was maintained constant ($\omega_0 = 3.8$). The reducing agent (NaBH_4) was added to the micellar solution as solid. After complete reduction that takes place in a few minutes, acetone was added to the solution to cause phase separation. The precipitate formed by the metallic nanoparticles was washed several times with acetone in order to eliminate surfactant molecules and finally kept in ultra-pure water as a suspension.

X-ray diffraction (XRD) patterns were obtained with a Phillips PW1710 using a Cu $\text{K}\alpha$ source. The angular resolution in the 2θ -scans was 0.05° . The sample for X-ray analysis was prepared after phase separation and washed with acetone. X-ray photoelectron spectroscopy (XPS) measurements were performed with a VG-Microtech Multilab, using a Mg $\text{K}\alpha$

(1253.6 eV) source. Spectra were obtained with a constant pass energy of 50 eV. The pressure in the analysis chamber of the spectrometer was 5×10^{-10} mbar during the measurements. The BE values were obtained using a *Peak-fit Program*. Transmission electron microscopy (TEM) experiments were performed with a JEOL, JEM-2010 microscope working at 200 kV. The sample for TEM analysis was obtained by placing a drop of the dispersed solution onto a Formvar-covered copper grid and evaporating it in air at room temperature. The images were analysed with the analySIS 3.0 program. For each sample, usually over more than 300 particles from different parts of the grid were used to estimate the mean diameter and size distribution of the nanoparticles. Energy dispersive analysis by X-rays (EDAX) was obtained with a OXFORD, INCA model system.

2.2. Preparation of the electrodes and electrochemical measurements

The procedure used for the electrochemical study has been previously reported [25,28–30]. Briefly, as a current collector a polycrystalline gold disc electrode (5 mm diameter) on which nanoparticles were deposited was used. Metal nanoparticles were transferred to the gold collector by depositing a drop (generally 5–10 μL) of the nanoparticle water suspension on the surface of the gold disc. The counter electrode was a gold wire. Potentials were measured against a reversible hydrogen electrode (RHE) connected to the cell through a Luggin capillary. Potentials are quoted versus this reference electrode. All the electrochemical measurements were performed in a 0.5 M H_2SO_4 solution at room temperature. Electrolyte solutions were prepared with Milli-Q[®] water and Merck “suprapur” sulphuric acid every day an experiment was carried out. Solutions were de-oxygenated by bubbling Ar during 20 min. The electrode potential was controlled using a PGSTAT30 AUTOLAB system. CO adsorption on the electrodes was carried out by bubbling CO gas for 2 min at 0.03 V. After that, CO was removed from the solution by bubbling argon for 10 min. Before each experiment, the gold collector was mechanically polished with alumina and rinsed with ultra-pure water to eliminate the nanoparticles from previous experiments. Methanol oxidation voltammograms and chronoamperometric experiments were carried out in a 0.5 M $\text{H}_2\text{SO}_4 + 0.1$ M MeOH solution at room temperature. The methanol electrooxidation currents were normalized to the total moles of Pt + Ru used on the experiments. The methodology employed was similar to that previously reported in reference [30]. Very briefly, the metal loading was determined from the concentration of the original solution containing the nanoparticles which was calculated using ICP analysis. Moreover and in a similar way that in reference [30], the stability of the nanoparticles deposited was analyzed by plotting the adsorption charge of the nanoparticles versus volume added. The linearity found is the proof of this stability (see reference [30] for the case of PtPd nanoparticles).

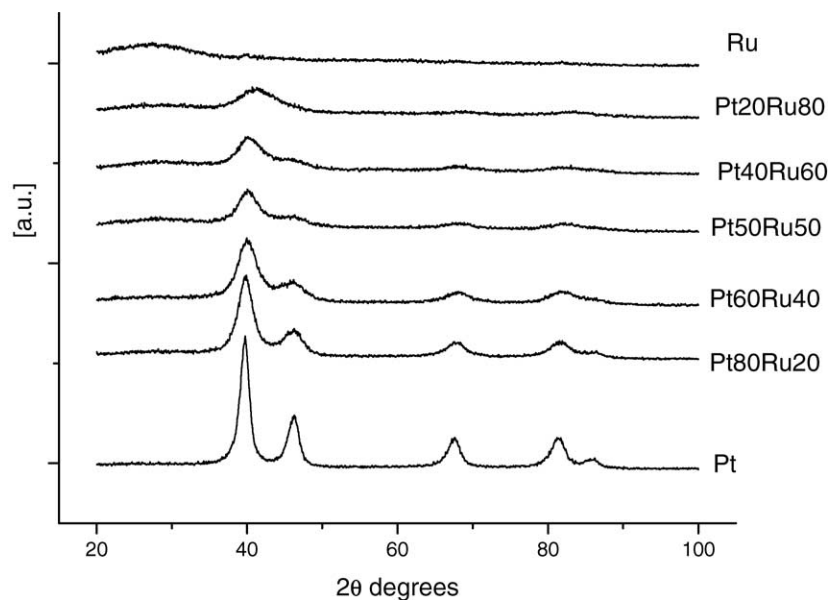


Fig. 1. XRD patterns of Pt/Ru nanoparticles.

3. Results and discussion

3.1. XRD, XPS and TEM/EDAX analyses

Cu $K\alpha$ X-ray diffraction patterns of PtRu nanoparticles are shown in Fig. 1. In the case of pure Pt, the diffraction peaks of a face centered cubic structure can be observed. For PtRu nanoparticles, a shift to higher 2θ values and an increase of peak broadening, with respect to the diffraction lines of pure Pt, were observed as the nominal content of Ru increases, indicating a decrease of both lattice parameter and mean particle size [31]. However a gradual loss of signal is clearly detected as the amount of Ru increases, which could indicate

that only part of the Ru is present as PtRu alloy remaining the other part in an amorphous state. No presence of hexagonal structure has been detected. Despite this loss of crystallinity, a linear relationship between lattice parameter, calculated with Vegard's law, and bulk composition is found with Ru concentrations of less than 60 at.% according to the phase diagram for Pt–Ru alloys, Fig. 2. Watanabe et al. [32] and Gasteiger et al. [33] have previously reported similar results.

To get information on surface composition and oxidation states of Pt and Ru, a XPS analysis was carried out. As an example, the Pt 4f spectrum obtained for Pt₅₀Ru₅₀ nanoparticles is reported in Fig. 3a. The Pt 4f signal in all the samples derives from the contribution of a single doublet

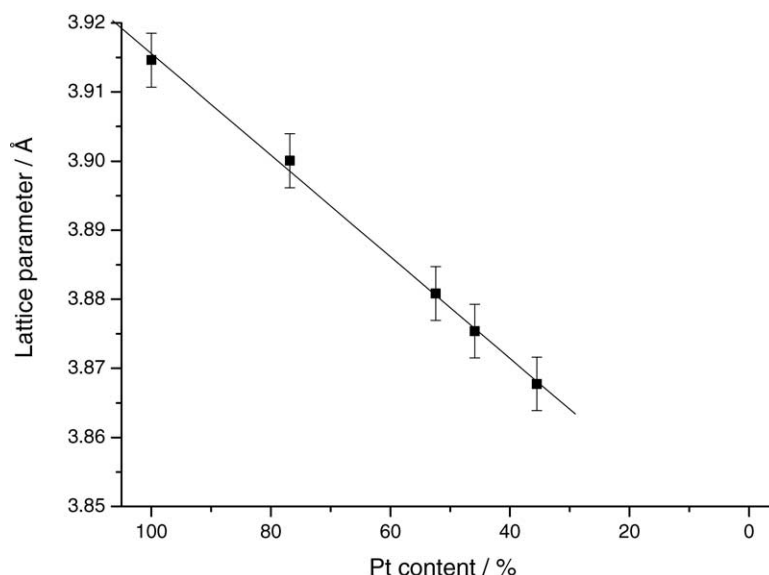


Fig. 2. Lattice parameter for Pt/Ru nanoparticles deduced from XRD.

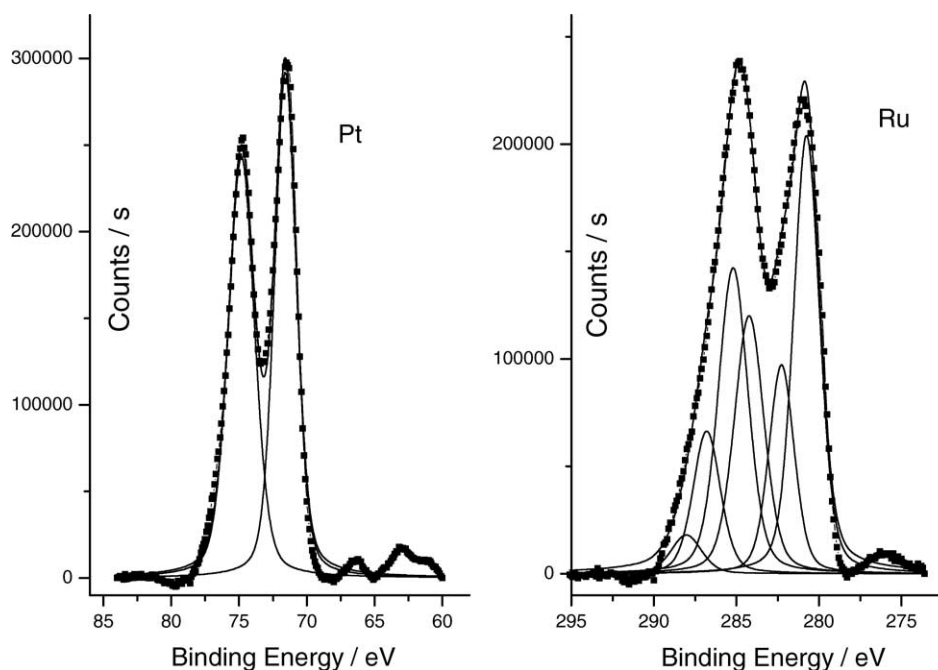


Fig. 3. XPS spectra for Pt₅₀Ru₅₀ nanoparticles.

except for the case of Pt₈₀Ru₂₀ (nominal) where a small contribution of a second doublet is also observed. The Pt 4f_{7/2} line occurs at a binding energy (BE) of 71.4 ± 0.3 eV assigned to Pt(0). In the case of Pt₈₀Ru₂₀ (nominal), the second doublet occurs at BE of 72.7 ± 0.3 eV assigned to Pt(II) species. The relative concentration of this PtO is around 18%. Very small differences are observed in terms of BE as a function of Ru concentration, suggesting that there is no strong modification of the electronic environment of Pt surface site with the change of the composition of the nanoparticles.

Despite the interference of C1s signal, the Ru species were studied by analysing the Ru 3d_{5/2} line. The spectrum corresponding to Pt₅₀Ru₅₀ nanoparticles is shown in Fig. 3b. In all the samples, Ru 3d_{5/2} derives from the contribution of two doublets at different binding energies. The highest BE peak (282.3 ± 0.3 eV) is related to oxidized Ru(IV) species, whereas the lowest BE species (280.8 ± 0.3 eV) are mainly due to metallic and/or lower oxidation state of Ru species [34–36]. For PtRu alloys, the high BE species have a relative concentration of $30 \pm 5\%$, whereas in the case of pure Ru, the relative concentration of these high BE species is around 60%. The other two peaks are associated with two different C species. One signal is due to the presence of residual surfactant on the surface of the nanoparticles (this residual surfactant was removed using our electrochemical cleaning protocol [29,30]) and the second one is associated with the atmospheric contamination of the sample.

XPS experiments were also used to calculate the atomic composition of PtRu nanoparticles (Table 1) by integration of the Pt and Ru deconvoluted signal and the atomic

sensitivity factor of Pt and Ru. As it can be observed, the calculated atomic compositions are very close to the nominal composition of the nanoparticles. These results show the effective control on the nanoparticle composition. In this point, it is important to note that XPS measurements are generally used to determine the surface composition. However, in electrocatalyst this XPS surface concentration corresponds to a thicker layer than that that takes part in the electrochemical reaction. Thus, these XPS experiments could only give us some indications about the surface composition.

TEM/EDAX analyses were performed to measure both particle size and atomic composition. Fig. 4 shows the mean particle size in the whole range of Pt and Ru concentrations. In all cases an average particle size of around 4 ± 1 nm was found. These results are in agreement with the fact that ω_0 was maintained constant for the synthesis of the nanoparticles. EDAX experiments were carried out in three different regions of the sample and the results are summarized in Table 2. As it was previously shown for XPS experiments, the calculated atomic compositions of the nanoparticles correspond with the nominal ones.

Table 1
Quantitative XPS data for Pt/Ru nanoparticles

Nominal atomic composition (Pt/Ru)	Band observed	Calculated atomic composition (Pt/Ru)
80/20	Pt 4f _{7/2} Ru 3d _{5/2}	76.8/23.2
60/40	Pt 4f _{7/2} Ru 3d _{5/2}	52.4/47.6
50/50	Pt 4f _{7/2} Ru 3d _{5/2}	45.9/54.1
40/60	Pt 4f _{7/2} Ru 3d _{5/2}	35.5/64.5
20/80	Pt 4f _{7/2} Ru 3d _{5/2}	18.7/81.3

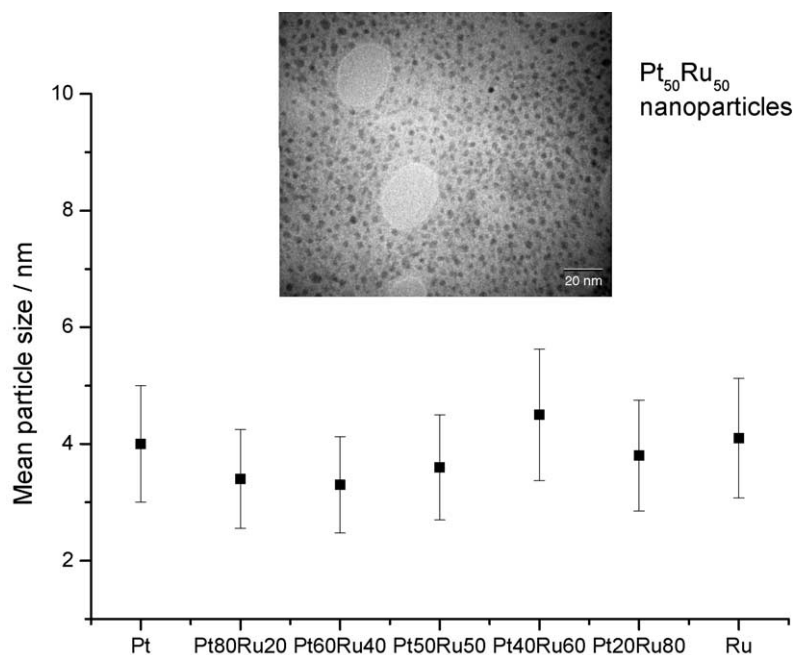


Fig. 4. Mean particle size of Pt/Ru nanoparticles vs. atomic composition. TEM image of Pt₅₀Ru₅₀ nanoparticles.

3.2. Electrochemical characterization

3.2.1. Voltammetry and CO_{ad} oxidation on PtRu nanoparticles

The decontamination procedure used to remove the surfactant layer from the surface of the nanoparticles was described in previous papers [29,30]. Very briefly, after the deposition of the nanoparticles on the gold support, the electrode was immersed into the sulphuric acid solution and a constant potential of 0.03 V was applied for 3 min. After that, the potential was stepped to 0.05 V and to observe the surface condition several voltammograms were recorded between 0.05 and 0.4 V. This procedure was repeated at least three times. After that and to improve the surface cleanliness of the electrode, CO was adsorbed on the nanoparticles holding the electrode at a potential of 0.03 V and bubbling CO into the solution during 2 min. After that, the CO was electrochemically stripped from the surface.

The voltammograms of clean Pt, Ru and Pt/Ru nanoparticles can be observed in Fig. 5. Since at potentials above 0.9–0.95 V corrosion and loss of Ru have been reported [37,38], we have limited the positive upper

potential to 0.8 V. In the case of Pt nanoparticles the voltammetric profile is characteristic of clean surfaces, showing the very well-known adsorption states. Increasing the Ru composition, the so-called hydrogen region appears structureless and an increase of the charge in the double layer region is also observed. This increase in the double layer region current has been previously described and it has been even used to estimate the amount of Ru for platinum single crystals decorated by spontaneous deposition with Ru [39,40]. Moreover, the voltammetric profile of the different PtRu nanoparticles is similar to those previously reported [5,8,11,41–44]. Only in the case of pure Ru it is necessary to point out that in our voltammogram no signal of adsorbed hydrogen is observed. This result is different to those from other works where a clear hydrogen adsorption region can be seen [5,7,8,42,45]. The absence of this region could be explained taking into account the amorphous state of our Ru nanoparticles as it was shown in XRD experiments.

CO adsorption–oxidation may be quantitatively used as a composition and structure sensitive surface probe [46]. In this way, Figs. 6 and 7 show the CO stripping on PtRu nanoparticles and the correlation between atomic composition and CO stripping peak potential, respectively.

CO stripping on pure Pt (Fig. 6a) leads to a shoulder at approximately 0.5 V and two main peaks at 0.72 and 0.76 V. Whereas the shoulder has been correlated with the oxidation of bridge-bonded CO [47], the multiplicity in the main oxidation current has been attributed to contributions from different crystalline orientations [46,48]. Similar peaks have been also found on low-index Pt single crystal surfaces, with slightly different peak potentials for the different orientations [49–51].

Table 2

Atomic composition of Pt/Ru nanoparticles from EDAX experiments

	Sample-1	Sample-2	Sample-3
Pt	Pt100	Pt100	Pt100
Pt80Ru20	Pt78.5Ru21.5	Pt77.1Ru22.9	Pt80.8Ru19.2
Pt60Ru40	Pt60.5Ru39.5	Pt60.5Ru39.5	Pt59.7Ru40.3
Pt50Ru50	Pt47.9Ru52.1	Pt47.7Ru52.3	Pt43.5Ru56.5
Pt40Ru60	Pt38.3Ru61.7	Pt39.9Ru60.1	Pt42.2Ru57.8
Pt20Ru80	Pt20.6Ru79.4	Pt18.7Ru81.3	Pt20.0Ru80.0
Ru	Ru100	Ru100	Ru100

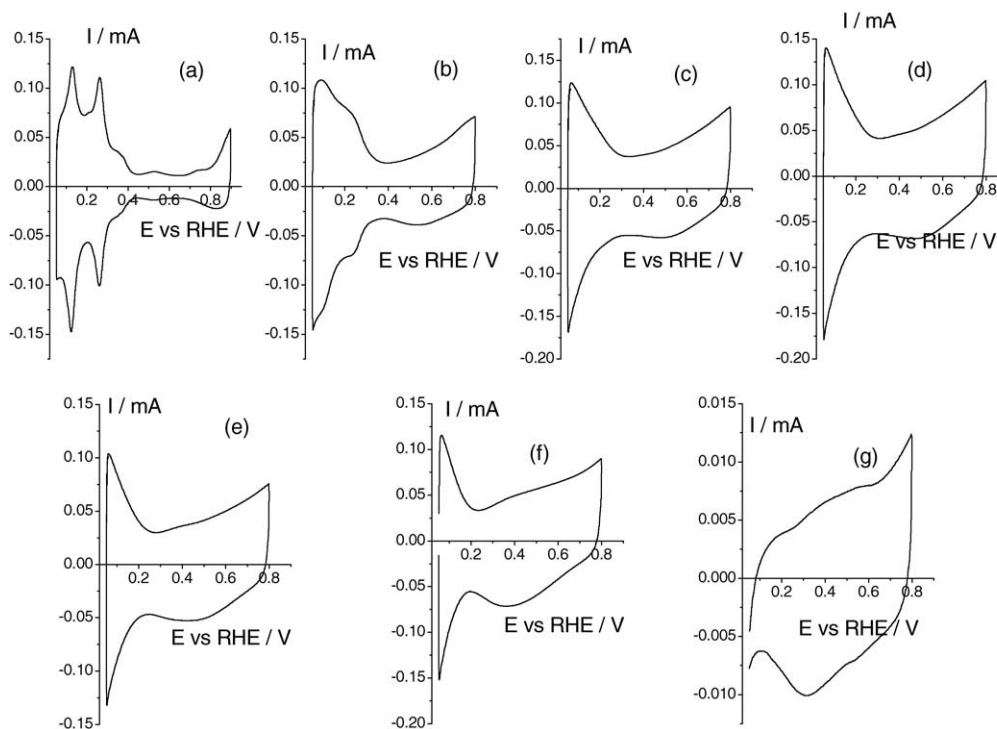


Fig. 5. Voltammograms of (a) Pt, (b) Pt₈₀Ru₂₀, (c) Pt₆₀Ru₄₀, (d) Pt₅₀Ru₅₀, (e) Pt₄₀Ru₆₀, (f) Pt₂₀Ru₈₀ and (g) Ru nanoparticles. Test solution, 0.5 M H₂SO₄; sweep rate, 20 mV s⁻¹.

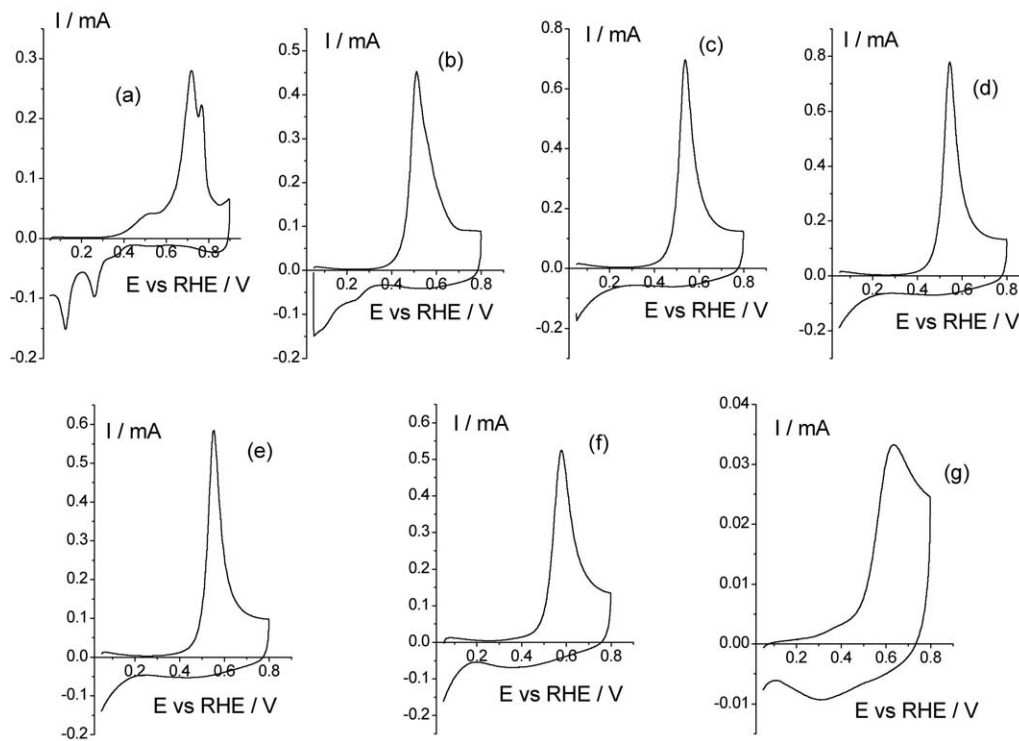


Fig. 6. CO stripping on (a) Pt, (b) Pt₈₀Ru₂₀, (c) Pt₆₀Ru₄₀, (d) Pt₅₀Ru₅₀, (e) Pt₄₀Ru₆₀, (f) Pt₂₀Ru₈₀ and (g) Ru nanoparticles. Test solution, 0.5 M H₂SO₄; sweep rate, 20 mV s⁻¹.

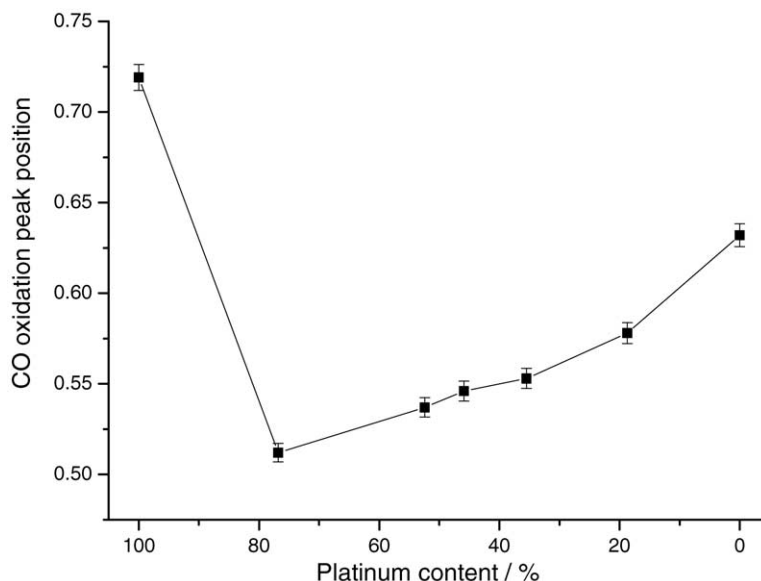


Fig. 7. CO oxidation peak potential vs. atomic Pt percentage in the nanoparticles. Test solution, 0.5 M H_2SO_4 ; sweep rate, 20 mV s^{-1} .

With only a 20% of Ru in the catalyst, a very clear negative shift (approximately 0.2 V compared with pure Pt) on the CO stripping peak can be observed. This shift has also been observed in previous studies [5,11]. Increasing the Ru concentration, the voltammetric profile of the CO oxidation remains quite similar but the CO stripping peak potential shifts to more positive values (Fig. 7). This tendency is different to that reported in other studies. For example, while with sputter-cleaned PtRu alloys the lowest potential for the oxidation of CO has been obtained for $\text{Pt}_{50}\text{Ru}_{50}$ [5], with PtRu alloy nanoparticles, the CO oxidation peak potential remains practically constant from 20 to 60% of Ru [11]. The differences found could be associated with a different surface atomic composition as a result of the different methods of synthesis. Moreover, it should be pointed out that CO oxidation is a structure sensitive reaction and nanoparticles synthesized by different means may have different surface structure [52,53].

In the case of pure Ru, a single broad oxidation peak at 0.63 V is found. It is important to note that, although the voltammetric profile in absence of adsorbed CO (Fig. 6g) was different to that previously published [5,7,8,42,45], the voltammetric profile of CO stripping is very similar to that reported [5,7,8,33]. The absence of this “so-called” hydrogen adsorption/desorption region could be related to the existence of Ru species in an amorphous state, according to the XRD results.

3.2.2. Methanol oxidation on PtRu nanoparticles

It is widely accepted that PtRu is the most promising binary electrocatalyst for methanol oxidation. Its superior activity has been observed for different PtRu materials, such as PtRu alloys [3,6,7], PtRu electrodeposits [42], Ru electrodeposits on Pt [39] and Ru adsorbed on Pt single-crystal [10] and on Pt carbon supported electrodes [54].

Fig. 8 shows the methanol oxidation voltammograms for PtRu nanoparticles prepared in microemulsion. For a better comparison of the electrocatalytic activity of the different PtRu nanoparticles, it is necessary to rationalize their activities. In this aspect, several groups have used the “so-called” hydrogen adsorption/desorption process to calculate the surface area of the electrode. This method, which works well for Pt surfaces, is not suitable for PtRu due to the poorly separated underpotential and overpotential hydrogen evolution regions and specially by the presence of an undefined double layer contribution. On the other hand, CO stripping has been also used as a method to determine the surface area of PtRu nanoparticles [11]. We have used the number of moles (Pt + Ru) of the particle, previously employed for PtPd nanoparticles [30], to rationalize the electrocatalytic activity. One of the interests in this way of presenting the experimental data is to cancel the difference in atomic mass between Pt and Ru. This way of rationalizing is obviously different to that typically used in fuel cell electrode characterization (activity per 1 mg metal of catalyst).

For pure Pt the methanol oxidation voltammetric profile is very well-known and it has been reported for massive and high surface area Pt electrodes [7,55]. In our case, the upper potential of the cycle was limited to 0.9 V to avoid the reorganization of the surface Pt atoms of the nanoparticle, what will be described in more detail in a forthcoming publication [56]. When the methanol oxidation on pure Pt is compared with the oxidation on PtRu nanoparticles of different compositions (Fig. 8), some important features should be mentioned. The “molar oxidation current” decreases continuously as the Ru composition increases. This decay seems to be due to the presence of higher amounts of Ru on the surface, which is inert for methanol dehydrogenation. However, the onset of the methanol oxidation shifts to lower potentials than for pure platinum. For

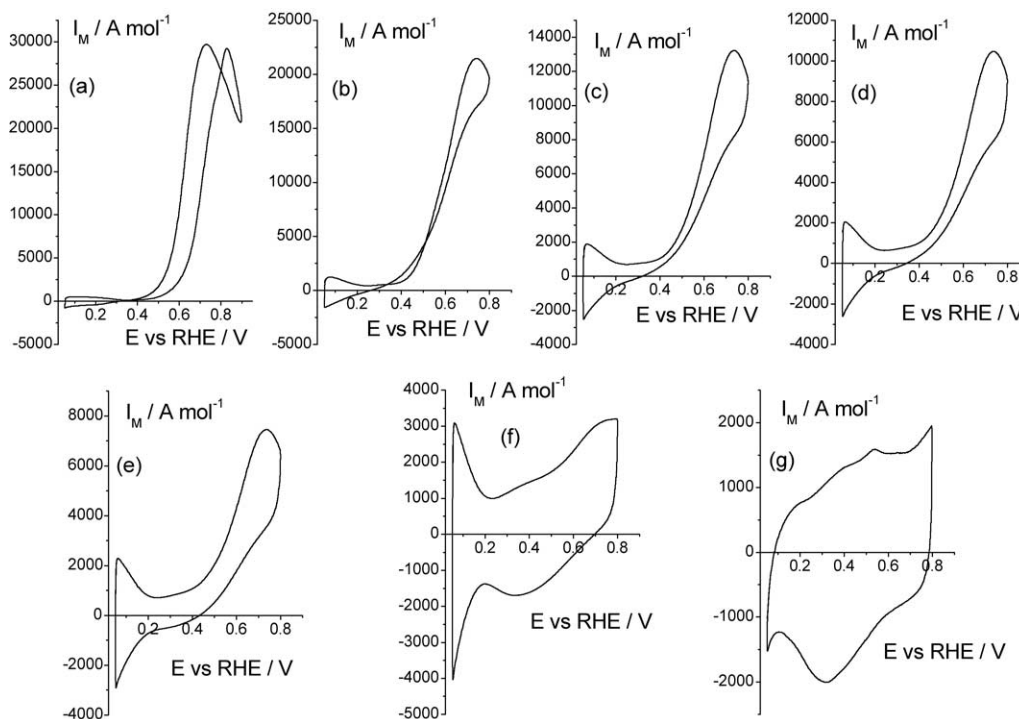


Fig. 8. Methanol electrooxidation on (a) Pt, (b) Pt₈₀Ru₂₀, (c) Pt₆₀Ru₄₀, (d) Pt₅₀Ru₅₀, (e) Pt₄₀Ru₆₀, (f) Pt₂₀Ru₈₀ and (g) Ru nanoparticles. Test solution, 0.5 M H₂SO₄ + 0.1 M MeOH; sweep rate, 20 mV s⁻¹.

the alloys, the peak (positive scan) potential remains practically constant (approximately 0.73 V) in the whole composition range. According to all these data, it is very difficult to choose the most active electrocatalyst for methanol oxidation. For this reason, chronoamperometric experiments with different potential steps were performed in a 0.5 M H₂SO₄ + 0.1 M MeOH solution at room temperature and at different electrode potentials. Fig. 9 resumes the results obtained after 200 s at room temperature. Thus, the highest

“molar oxidation currents” were obtained with Pt₈₀Ru₂₀ (nominal) independently of the applied potential and specially at potentials useful for a DMFC. PtRu nanoparticles with Pt ranging between 80 and 40% show higher oxidation currents than pure platinum. A similar tendency was obtained by Jusys et al. [11] where the oxidation current was normalised to the surface area calculated by DEMS. The nominal composition Pt₈₀Ru₂₀ also coincides with that given by Gasteiger et al. [7] (experimentally and by statistical

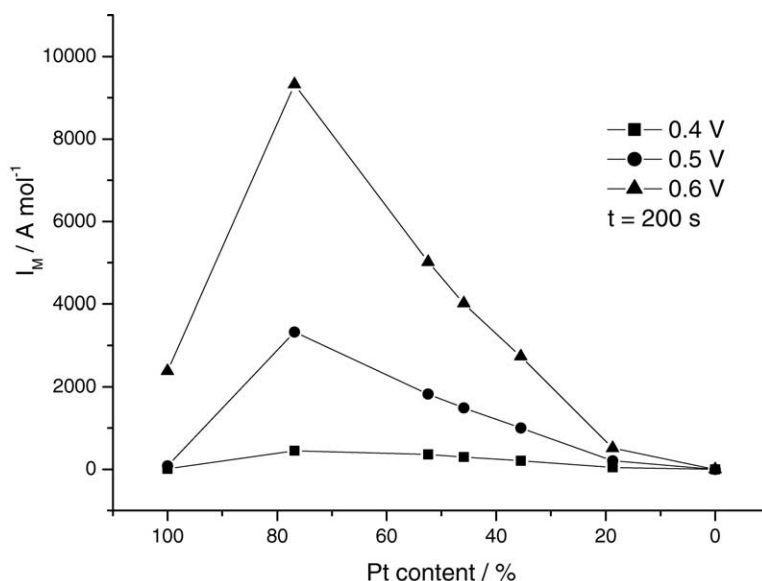


Fig. 9. “Molar current current” for methanol electrooxidation vs. alloy composition. Test solution, 0.5 M H₂SO₄ + 0.1 M MeOH solution.

calculus) for bulk Pt/Ru alloys. Finally it is important to recall that these experiments were performed at room temperature, which implies that similar experiments should be carried out at more elevated temperatures to evaluate the optimal atomic composition in these new conditions.

4. Conclusions

The microemulsion method can be used for synthesizing PtRu nanoparticles of different compositions being the electrocatalytic activity very similar to that obtained with other nanoparticles and bulk alloys synthesized using more complicated procedures. The method allows a very controlled change of composition still keeping constant the dimension of the nanoparticles. Given the characteristics of the synthesis, the scale-up of the process for obtaining bigger amounts of nanoparticles for industrial use should be easy. A controlled procedure allows cleaning the surface of the particles avoiding contamination and change of the surface structure. The nanoparticles have been physically characterized by different means. XRD experiments show the presence of PtRu alloys with a fcc structure. A very clear loss of signal is detected when the Ru concentration is increased and it has been attributed to the presence of Ru in an amorphous state. XPS has been used to determine the atomic composition of the nanoparticles, which is in agreement with the expected from the synthesis conditions. The nominal atomic composition was also confirmed by EDAX studies. The particle sizes of the PtRu nanoparticles in the whole range of composition are 4 ± 1 nm as determined by TEM.

PtRu nanoparticles were electrochemically characterized after a controlled decontamination procedure. Cyclic voltammetry of the different nanoparticles was obtained in sulphuric acid showing the characteristic voltammetric profile of clean nanoparticles. Only in the case of pure Ru, the voltammogram is different to that previously reported which may be due to the presence of amorphous Ru. CO_{ad} oxidation and methanol oxidation reactions were used to study some of the electrocatalytic properties of the PtRu nanoparticles. The results indicate that PtRu nanoparticles of 80:20 nominal atomic composition have the best performance at room temperature. In the case of methanol oxidation, the number of moles of both metals was employed applied to rationalise the data in order to get a better comparison of the electrocatalytic properties of the PtRu nanoparticles of different composition.

Acknowledgements

The authors acknowledge financial support from “Ministerio de Ciencia y Tecnología” project (BQU2003-03877) and from “Generalitat Valenciana” project (GRUPOS03/126). J. Solla-Gullón and F.J. Vidal-Iglesias are also grateful

to the “Ministerio de Ciencia y Tecnología”, Spain, for their research grant.

References

- [1] M. Watanabe, S. Motoo, *J. Electroanal. Chem.* 60 (1975) 267.
- [2] M. Watanabe, S. Motoo, *J. Electroanal. Chem.* 60 (1975) 275.
- [3] T. Iwasita, F.C. Nart, W. Vielstich, *Ber. Bunsenges. Phys. Chem.* 94 (1990) 1030.
- [4] T. Frelink, W. Visscher, J.A.R. van Venn, *Langmuir* 12 (1996) 3702.
- [5] H.A. Gasteiger, N. Markovic, P.N. Ross, E.J. Cairns, *J. Phys. Chem.* 98 (1994) 617.
- [6] A. Kabbabi, R. Faure, R. Durand, B. Beden, F. Hahn, J.M. Leger, C. Lamy, *J. Electroanal. Chem.* 444 (1998) 41.
- [7] H.A. Gasteiger, N. Markovic, P.N. Ross, E.J. Cairns, *J. Phys. Chem.* 97 (1993) 12020.
- [8] F. Richarz, B. Wohlman, U. Vogel, H. Hoffschulz, K. Wandelt, *Surf. Sci.* 335 (1995) 361.
- [9] T. Iwasita, H. Hoster, A. John-Anacker, W.F. Lin, W. Vielstich, *Langmuir* 16 (2000) 522.
- [10] W. Chzanowski, A. Wieckowski, *Langmuir* 13 (1997) 5974.
- [11] Z. Jusys, J. Kaiser, R.J. Behm, *Electrochim. Acta* 47 (2002) 3693.
- [12] A.J. Dickinson, L.P.L. Carrette, J.A. Collins, K.A. Friedrich, U. Stimming, *Electrochim. Acta* 47 (2002) 3733.
- [13] M. Boutonnet, J. Kizling, P. Stenius, G. Marie, *Colloids Surf.* 5 (1982) 209.
- [14] M.A. López-Quintela, J. Rivas, *J. Colloid Interface Sci.* 158 (1993) 446.
- [15] R. Tourode, P. Girard, G. Marie, J. Kizling, M. Boutonnet-Kizling, P. Stenius, *Colloids Surf.* 67 (1992) 9.
- [16] M.L. Wu, D.H. Chen, T.C. Hung, *Langmuir* 17 (2001) 3877.
- [17] J. Nagy, *Colloids Surf.* 35 (1989) 201.
- [18] K. Osseo-Asare, F.J. Arriagada, *Colloids Surf.* 50 (1990) 321.
- [19] E. Joselevich, I. Willner, *J. Phys. Chem.* 98 (1994) 7628.
- [20] V. Chhabra, M. Lal, A.N. Maitra, P. Ayyub, *Colloid Polym. Sci.* 273 (1995) 939.
- [21] C.L. Chang, H.S. Fogler, *AIChE J.* 42 (1996) 3153.
- [22] L. Liz, M.A. López-Quintela, J. Mira, J. Rivas, *J. Mater. Sci.* 29 (1994) 3739.
- [23] M. Singhal, V. Chhabra, P. Kang, D.O. Shah, *Mater. Res. Bull.* 32 (1977) 239.
- [24] M. Antonietti, R. Basten, S. Lohmann, *Macromol. Chem. Phys.* 196 (1995) 441.
- [25] J. Solla-Gullón, V. Montiel, A. Aldaz, J. Clavilier, *J. Electroanal. Chem.* 491 (2000) 69.
- [26] M.J. Escudero, E. Hontañón, S. Schwartz, M. Boutonnet, L. Daza, *J. Power Sources* 106 (2002) 206.
- [27] Y. Liu, X. Qui, Z. Chen, W. Zhu, *Electrochem. Commun.* 4 (2002) 550.
- [28] J. Solla-Gullón, V. Montiel, A. Aldaz, J. Clavilier, *Electrochem. Commun.* 4 (2002) 716.
- [29] J. Solla-Gullón, V. Montiel, A. Aldaz, J. Clavilier, *J. Electrochem. Soc.* 150 (2) (2003) 104.
- [30] J. Solla-Gullón, A. Rodes, V. Montiel, A. Aldaz, J. Clavilier, *J. Electroanal. Chem.* 554 (2003) 273.
- [31] A.S. Aricò, P.L. Antonucci, E. Modica, V. Baglio, H. Kim, V. Antonucci, *Electrochim. Acta* 47 (2002) 3723.
- [32] M. Watanabe, M. Uchida, S. Motoo, *J. Electroanal. Chem.* 229 (1987) 395.
- [33] H.A. Gasteiger, N. Markovic, P.N. Ross, E.J. Cairns, *Surf. Sci.* 67 (1993) 293.
- [34] J.B. Goodenough, R. Manoharan, A.K. Shukla, K.V. Ramesh, *Chem. Mater.* 1 (1989) 391.
- [35] A.S. Aricò, P. Creti, H. Kim, R. Mantenga, N. Giordano, V. Antonucci, *J. Electrochem. Soc.* 143 (1996) 3950.

- [36] A.S. Aricò, G. Monforte, E. Modica, P.L. Antonucci, V. Antonucci, *Electrochem. Commun.* 2 (2000) 466.
- [37] S. Hadzi-Jordanov, H. Angerstein-Kozłowska, M. Vukovic, B.E. Conway, *J. Phys. Chem.* 125 (1978) 1471.
- [38] B. Beden, F. Kardigan, C. Lamy, J.M. Leger, *J. Electroanal. Chem.* 127 (1981) 75.
- [39] W. Chzanowski, A. Wieckowski, *Langmuir* 14 (1998) 1963.
- [40] W. Chzanowski, H. Kim, A. Wieckowski, *Catal. Lett.* 50 (1998) 69.
- [41] C. Pan, F. Dassenoy, M.J. Casanove, K. Philippot, C. Amiens, P. Lecante, A. Mosset, B. Chaudret, *J. Phys. Chem. B* 103 (1999) 10098.
- [42] M. Krausa, W. Vielstich, *J. Electroanal. Chem.* 379 (1994) 307.
- [43] U.A. Paulus, U. Enduschat, G.J. Feldmeyer, T.J. Schmidt, H. Bönemann, R.J. Behm, *J. Catal.* 195 (1999) 383.
- [44] C. Roth, N. Martz, F. Hahn, J.M. Leger, C. Lamy, H. Fuess, *J. Electrochem. Soc.* 149 (2002) 433.
- [45] H.N. Dinh, X. Ren, F.H. Garzon, P. Zelenay, A. Gottesfeld, *J. Electroanal. Chem.* 491 (2000) 222.
- [46] B. Beden, C. Lamy, N.R. De Tacconi, A.J. Arvia, *Electrochim. Acta* 35 (1990) 691.
- [47] A.M. Castro Luna, N.C. Giordano, A.J. Arvia, *J. Electroanal. Chem.* 34 (1975) 97.
- [48] A.M. De Becdelièvre, J.J. De Becdelièvre, J. Clavilier, *J. Electroanal. Chem.* 294 (1990) 97.
- [49] J.M. Feliu, J.M. Orts, A. Fernández-Vega, A. Aldaz, *J. Electroanal. Chem.* 296 (1990) 191.
- [50] E. Herrero, J.M. Feliu, A. Aldaz, *J. Electroanal. Chem.* 368 (1994) 101.
- [51] B.E. Hayden, A.J. Murria, R. Parsons, D.J. Pegg, *J. Electroanal. Chem.* 409 (1996) 51.
- [52] T.S. Ahmadi, Z.L. Wang, T.C. Green, A. Henglein, M.A. El-Sayed, *Science* 272 (1996) 1924.
- [53] T.S. Ahmadi, Z.L. Wang, A. Henglein, M.A. El-Sayed, *Chem. Mater.* 8 (1996) 1161.
- [54] P. Waszczuk, J. Solla-Gullón, H.S. Kim, Y.Y. Tong, V. Montiel, A. Aldaz, A. Wieckowski, *J. Catal.* 203 (2001) 1.
- [55] Z. Jusys, R.J. Behm, *J. Phys. Chem. B* 105 (2001) 10874.
- [56] J. Solla-Gullón, A. Aldaz, J. Clavilier, in preparation.